Available online at www.sciencedirect.com

jmr&t Journal of Materials Research and Technology

https://www.journals.elsevier.com/journal-of-materials-research-and-technology

Original Article

Austenite grain growth and hot deformation behavior in a medium carbon low alloy steel

A. Chamanfar[a,*], S.M. Chentouf[a], M. Jahazi[a], L.-P. Lapierre-Boire[b]

[a] Département de Génie Mécanique, École de Technologie Supérieure, 1100 rue Notre-Dame Ouest, Montréal, Québec, H3C 1K3, Canada
[b] Finkl Steel-Sorel Inc., 100 McCarthy, Saint-Joseph-de-Sorel, Québec, J3R 3M8, Canada

ARTICLE INFO

Article history:
Received 1 July 2020
Accepted 28 August 2020
Available online 15 September 2020

Keywords:
Medium carbon low alloy steel
Austenitization
Austenite grain growth
Hot deformation
Flow stress
Grain refinement

ABSTRACT

To examine the austenite grain growth behavior and kinetics under isothermal austenitization process in a low alloy medium carbon forged steel, heat treatments at different temperatures (1150, 1175, 1200, and 1260 °C) and times (5, 15, and 25 min) were conducted. An Arrhenius constitutive relationship was developed to analyze and predict the austenite grain size as a function of the austenitization temperature and time during isothermal austenitization. The model predictions agreed well with the experimental austenite grain size data. Following the austenitization examinations, the hot deformation behavior of the alloy was studied by performing isothermal compression tests for different soaking times (5, 15, and 25 min) at the deformation temperatures of 1150, 1175, and 1200 °C, at a constant strain rate of 0.05 s^{-1}, and up to a true strain of 0.6. The microstructures of the hot compressed samples were assessed to determine the dynamic softening mechanisms and potential austenite grain refinement by dynamic recrystallization (DRX). Under the investigated hot deformation conditions, the flow stress curves and microstructure observations showed DRX characteristics. The flow curves from the peak to the steady-state stress were accurately predicted using a Johnson–Mehl–Avrami–Kolmogorov (JMAK) equation. Based on the flow curves and a mathematical equation, the DRX kinetics were also determined. Variations of the flow curves, DRX kinetics, and dynamic recrystallized (DRXed) grain size with the deformation temperature, strain, and the austenite grain size prior to deformation were analyzed.

1. Introduction

Medium carbon low alloy steels are widely used in automotive (*e.g.*, gears and crankshafts) and aerospace (*e.g.*, plastic injection molds) industries as well as for fabrication of high-end safety parts as molds materials because of their high strength, satisfactory fracture toughness, long fatigue life, and adequate stress corrosion resistance [1–5]. In manufacturing sequence of these alloys, the hot forged slab produced from a cast ingot enters an austenitization furnace and is soaked for a specific time, then it is passed to a hot forging mill. Soaking temperature and time during austenitization are primary controlling variables in the hot forging process [6]. They affect austenite grain growth and dissolution of precipitates. Therefore, they control prior austenite grain size, austenite recrystallization and refinement, phase transformation, and amount of carbides/carbonitrides precipitation during hot forging and subsequent cooling from hot forging tempera-

* *Corresponding author.*
E-mail: ahmad.chamanfar@mail.mcgill.ca (A. Chamanfar).
https://doi.org/10.1016/j.jmrt.2020.08.114

tures and thus, the mechanical properties [3,6,7]. For instance, coarse initial austenite grain size makes the grain refinement during hot forging more challenging [7]. Besides difficulty in microstructure control, coarse prior austenite grains lead to defect formation during hot forging such as surface cracking along austenite grain boundaries [8]. As well, a coarse austenite grain size moves the continuous cooling transformation curve to the right, thus enhancing the chance of martensite formation [9]. Therefore, controlling and predicting the prior austenite grain size is necessary to attain sound mechanical properties.

Studies on austenite grain growth during austenitization prior to hot deformation in different steel grades have been conducted, though in many studies the focus has been mostly on the impact of alloying elements [10–12]. In thermomechanical processing of different steels, austenite grain growth is controlled by addition of alloying elements. In this way, through solute drag effects and/or Zener pinning of austenite grain boundaries by fine carbides or carbonitrides precipitates, a satisfactory balance between strength, toughness, ductility, formability, and weldability is created through attaining a fine microstructure [9–11,13]. Yu et al. [12] studied Nb role on austenite grain growth in a low-carbon steel and indicated that in the 1150–1230 °C soaking temperature range, austenite grains in 0.015% Nb steel are finer than those of Nb free steel. Some studies on the impact of the initial grain size before austenitization as well as the soaking temperature and time in the austenitization process on austenite grain growth are available in literature. Duan et al. [6] pointed out that the austenite grains grow with increasing the austenitization temperature and time in the X80 pipeline steel. As well, Chen et al. [14] and Liu et al. [15] indicated that in different steel grades with increasing the initial grain size, the rate of austenite grain growth during austenitization decreases. Also, some theoretical and empirical models and equations based on austenitization temperature and time mostly for plain carbon–manganese, dual phase, high-strength low-alloy (HSLA) steels and rarely on medium carbon low alloy steels have been proposed to quantify the austenite grain growth kinetics during austenitization [11,16].

Depending on the processing conditions, the medium carbon low alloy steels can exhibit a high deformation resistance at elevated temperatures [1]. As well, applying small reductions during hot deformation make the austenite grain refinement more challenging [7]. Moreover, in these alloys, the tendency for grain coarsening during hot deformation processes adversely affects the final mechanical properties [1,2]. Also, many medium carbon low alloy steels may not require final heat treatment after hot forging [17]. Thus, it is essential to investigate, control, and optimize the hot deformation process parameters to obtain sound products. For instance, refinement of prior austenite grains during hot deformation through DRX incidence (austenite conditioning) followed by accelerated cooling is an important approach to improve both strength and toughness at the same time. This is feasible by controlling the hot deformation process parameters [18,19].

In literature, the hot deformation behavior of several medium carbon low alloy steels such as the conventional grade, *i.e.,* AISI 4140 (in wt.% 0.40 C–0.67 Mn–0.21 Si–0.97 Cr–0.15 Mo–0.045 P–0.030 S–balance Fe) [20] and other grades like VCN200 [21] is investigated using isothermal compression testing. Wei et al. [22] indicated that the flow stress of the experimental 0.23 C–1.50 Mn–1.79 Al (wt.%) high strength steel increases with decreasing deformation temperature and increasing strain rate, as expected. During hot deformation of medium carbon low alloy steels, dynamic recovery (DRV), DRX, grain growth, and dynamic evolution of particles (precipitation, growth/coalescence, and dissolution,) can occur and affect the flow behavior, microstructure evolution, and mechanical properties.

However, the effect of austenitization prior to hot deformation on austenite grain growth has been rarely reported for medium carbon low alloy steels. Even though studies on grain growth have been carried out, more investigation is required on control and quantification of grain growth and its impact on microstructure evolution during hot deformation. To this end, in this study the effects of soaking temperature and time during austenitization on the austenite grain growth kinetics are assessed. As well, based on the experimental results an Arrhenius constitutive equation for predicting the growth behavior of austenite grains is proposed. The developed equation is validated by comparing the measured and predicted austenite grain sizes.

Similarly, less data is available in literature on the hot deformation characteristics of medium carbon low alloy steels compared with other grades like HSLA steels. Therefore, hot compression testing at different temperatures and prior austenite grain sizes at a fixed strain rate was carried out to study the hot deformation behavior of the alloy. The flow curves were evaluated regarding the related hardening and softening mechanisms for different hot deformation conditions. As well, the JMAK equation was used to predict the flow behavior of the alloy.

And finally, an in-depth understanding of the microstructure evolution during industrial hot deformation process is essential for design, simulation, and optimization purposes to obtain a uniform and fine grain structure for balanced mechanical properties. Accordingly, the microstructure of the hot compressed samples was examined for a better understanding of the hot deformation mechanisms occurring under different conditions. In particular, the behavior and kinetic of DRX as well as conditions for full DRX occurrence and refinement of the coarse grain structure developed during the austenitization process were examined. In this manner, the appropriate parameters for austenitization and hot forging practices of the alloy at industrial scale can be established while the number of full-scale testing can be reduced significantly. Also, the generated data from the austenitization process and the hot compression tests is useful as input data for thermomechanical models.

2. Experimental procedures

The investigation was carried out on a high strength medium carbon low alloy steel supplied by Finkl Steel- Sorel (Quebec, Canada) in the as-forged condition. The nominal chemical composition of this steel is provided in Table 1. The alloy has a P20 designation in the AISI system. A thick slice ($1200 \times 800 \times 10$ mm^3) extracted from an industrial size hot

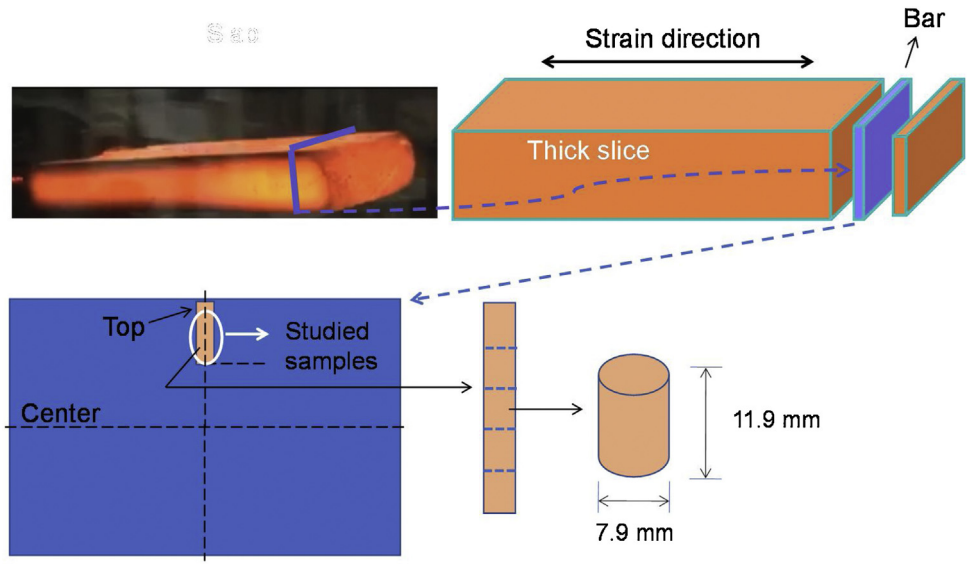

Fig. 1 – An image illustrating the initial slab, a thick slice from the slab, and extracting the austenitization and hot compression samples from a bar taken out from the thick slice.

Table 1 – Chemical composition of the studied steel in wt.%.

C	Mn	Si	Ni	Cr	Mo	Cu	Fe
0.37	0.84	0.39	0.25	1.87	0.46	0.16	Balance

forged rectangular slab (6000 × 1200 × 800 mm^3) was received. A bar (40 × 10 × 10 mm^3) was taken out perpendicular to the strain direction of the slab by electrical discharge machining. The location and orientation of the bar within the thick slice and the original slab is shown schematically in Fig. 1. For austenitization heat treatments and hot compression tests, cylindrical samples with a diameter of 7.9 mm and height of 11.9 mm were prepared from the bar (Fig. 1). The initial average grain size of these samples was determined as 100 ± 6 μm using the linear intercept method of ASTM E112-13 standard. These samples were divided in two sets: one set was used for austenitization heat treatments and the other set for hot compression tests.

A radiant cylindrical furnace installed on an MTS hot compression machine was used to carry out the austenitization heat treatments. The heating capability of the furnace was up to 1290 °C, and a K-type thermocouple in contact with the sample was used to accurately monitor and control the temperature during the tests. The samples and dies were enclosed in a quartz tube through which a constant flow of argon gas was circulated to increase the temperature homogeneity and minimize oxidation of samples and dies. The austenitization heat treatments were conducted at a 1 °C/s heating rate at different isothermal soaking temperatures (1150, 1175, 1200, and 1260 °C) for different soaking times (5, 15, and 25 min) followed by rapid water quenching to preserve the developed austenite grain structure. The investigated austenitization conditions are representative of the practical operation applied on the slab, after converting the initial ingot into a slab by hot forging.

For the austenitized samples, microstructural observations were conducted on the cylindrical basis. After conventional grinding and polishing, the austenite grain boundaries in austenitized samples were revealed by immersion chemical etching for 15–25 s in Villela's etchant composed of 1 g picric acid, 5 mL HCl, and 100 mL ethanol. Observations were made with Olympus DSX-500 opto-digital microscope. Average austenite grain size was measured based on the linear intercept method of the ASTM E112-13 standard and with the aid of a metallography quantitative image processing (MIP®) software considering at least five fields of view for every sample. In this way, more than 250 grains were counted for every sample to ensure representative average austenite grain size data. From the austenitized samples the relationships of the average austenite grain size to the austenitization temperature and time as well as the kinetics of the austenite grain growth were determined. In addition, the grain size data was implemented in a grain growth constitutive equation to predict the austenite grain size under different austenitization conditions.

On the second set of the samples prepared from the as-received material, uniaxial hot compression experiments at 1150, 1175 and 1200 °C were performed to a true strain of 0.6 (corresponding to an engineering strain of 45%) at a fixed and constant strain rate of 0.05 s^{-1}, followed by immediate water quenching to preserve the hot deformed microstructure. Before starting the compression, the samples were soaked at the deformation temperature for different times, *i.e.,* 5, 15, and 25 min, to investigate the impact of the prior austenite grain size on the hot deformation behavior. Also, by holding at the deformation temperature for these specific times, a uniform temperature throughout the samples was attained before compression by eliminating thermal gradients. Again, these hot deformation parameters are close to those experienced by the material during industrial hot forging of the slab after austenitization. In practice, an important stage prior to

forging is heating the slab to the forging temperature which along with the holding time must be carefully controlled. This is normally performed at high temperatures for a sufficient holding time to obtain a homogenous austenite and to make the material easy to forge.

For the hot compression tests, a computer controlled 100 kN servo-hydraulic MTS testing machine equipped with the radiant cylindrical furnace discussed above was used. The heating cycle of the hot compression tests was similar to that of the austenitization heat treatments in terms of heating rate, placing a thermocouple in contact with the sample for accurate temperature control, and circulating argon gas in the quartz tube containing the dies and the sample. During hot compression tests, graphite powder and mica sheet were used as lubricant layers between the both ends of the sample and the dies to reduce the friction and make the deformation more uniform throughout the sample. The load-displacement data recorded by the computer controller during the hot compression testing was converted to the true stress- true strain curves using standard methods. The effects of prior austenite grain size, deformation temperature, and strain on the flow stress were analyzed. A JMAK equation was used to predict the flow stress curves from the peak to the steady-state region, *i.e.,* the flow softening part of the curve. Additionally, the DRX kinetics were determined from the flow stress curves using conventional kinetics equations.

For metallographic analysis, the quenched hot compression samples were sectioned parallel to the compression axis at mid-diameter. Microstructure was examined at the center of the hot compressed samples. The metallography sample preparation and microstructure observations for the hot compressed samples were the same as the austenitized samples. For hot compression samples it was ensured that as a minimum, 250 grain intersections were considered for every sample. As well, the occurrence of DRX and refinement of the prior austenite grains and their evolution with temperature, strain, and prior austenite grain size were among the main objectives of the microstructure investigation in the hot compressed samples.

3. Results and discussion

3.1. *Effect of soaking temperature and time on austenite grain growth behavior*

As a representative example, an optical microscopy image for the microstructure examinations during austenitization heat treatments is provided in Fig. 2 for the steel sample quenched after soaking for 25 min at 1150 °C. The austenite grain structure of this sample reveals nearly equiaxed grains, almost hexagonal in shape, with flat grain boundaries. The grains are evidently coarsened during austenitization considering a starting grain size of $100 \pm 6\,\mu m$ and a final grain size of $388 \pm 9\,\mu m$ for this condition. The undissolved carbide particles are also visible. Quenching crack along the grain boundaries and martensite formation can be observed as well.

Based on the optical microscopy measurements, the average austenite grain size was quantitatively assessed as a function of the austenitization temperature and time. The

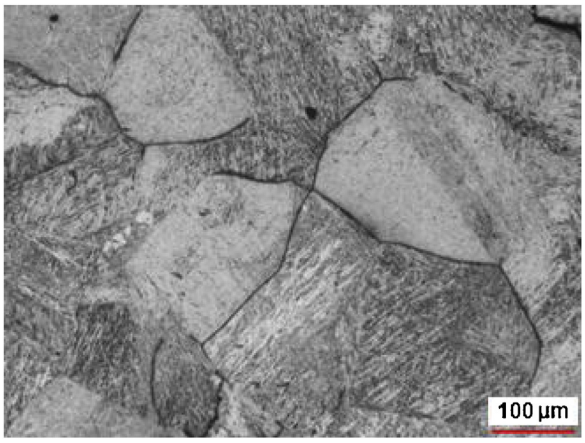

Fig. 2 – The austenite grain structure after austenitization at 1150 °C for 25 min.

variation of the austenite grain size with the austenitization temperature is depicted in Fig. 3a for different soaking times. Austenite grain size increases with the increasing of the soaking temperature, as expected. As well, the mechanism for austenite grain growth is grain boundary migration [14]. The driving force for the grain growth is reducing the grain boundary area per unit volume and thus, decreasing the free energy associated with the grain boundaries.

The grain boundary mobility increases with increasing temperature. In other words, grain boundary migration is a thermally activated process. As well, with increasing temperature, smaller amount of precipitates having relatively larger size (Fig. 2) are present and they are less effective in pinning the grain boundaries and inhibiting grain boundary migration or austenite grain growth. The sensitivity of the austenite grain size to the austenitization temperature is more pronounced for the soaking time of 25 min than 5 and 15 min. In the former, more time is available for coarsening of the precipitates which results in decreased pinning effect on the grain boundaries for inhibition of grain growth.

Referring back to Fig. 3a, the curves reach almost a plateau at the end, *i.e.,* after an adequately long period of isothermal soaking. This suggests that a limiting grain size is obtained. In other words, the grain growth comes to an end as a result of the existence of stable second phase particles like carbonitrides and solutes. Consequently, in a practical austenitization process, soaking time should be longer than 25 min to attain a steady prior austenite grain size and prevent variations in microstructure and mechanical properties in the component.

Effect of austenitization time on the average austenite grain size for different soaking temperatures is represented in Fig. 3b. At the soaking times equal or less than 15 min (900 s), the austenite grains grow slowly with the increase of the soaking time. In contrast, at longer soaking times (> 900 s) the austenite grain size increases faster, *i.e.,* growth rate is faster. In summary, austenite grain growth rate is initially slow and then increases as soaking time exceeds 15 min (900 s).

The chemical composition of the studied steel leads to carbides and/or carbonitrides formation that affects the growth of the austenite grains. Based on the Thermo-Calc. data [23], for

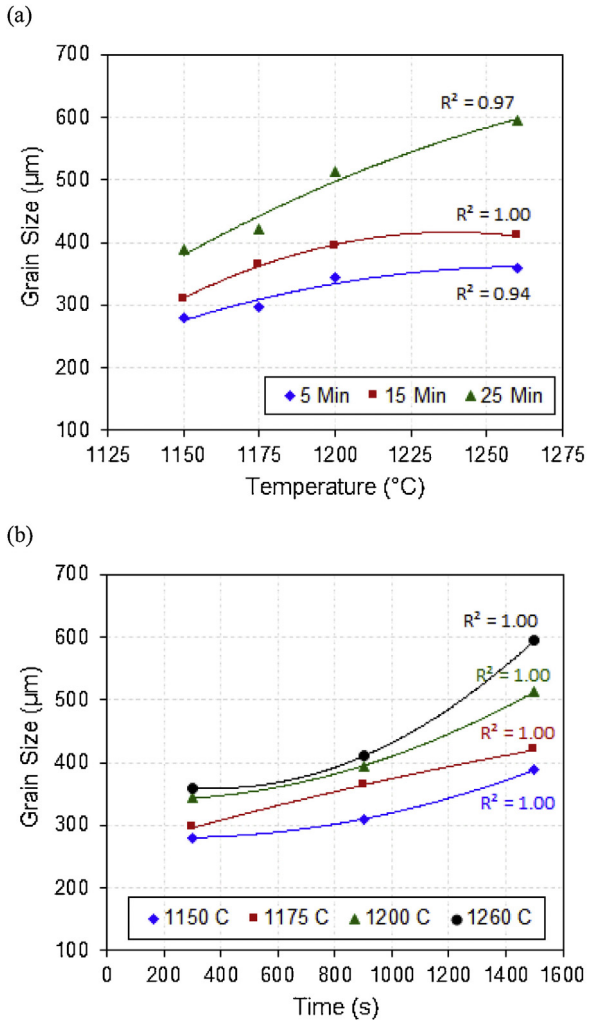

Fig. 3 – Variation of the average austenite grain size with the austenitization (a) temperature and (b) time.

chemical compositions close to the current steel, the equilibrium dissolution temperatures of different carbides including cementite (Fe_3C), $M_{23}C_6$, M_7C_3, M_6C, and M_3C_2 is below 900 °C. Here M indicates carbide former elements such as Cr and Mo in the investigated steel. From the above analysis, in the austenitization temperate ranges of this study (1150–1260 °C), these carbides should be in solution. Thus, only solutes by their dragging effect and carbonitrides stable up to temperatures close to the melting point of the alloy contribute in reducing the migration rate of the grain boundaries and thus, the grain growth. The alloying elements in solid solution in carbon steels act as barriers to austenite grain growth through segregation at austenite grain boundaries [11]. The difference in the atomic radii of an alloying element and Fe influences the solute dragging force on the grain boundaries [23]. X-ray mapping in scanning transmission electron microscope (STEM) has indicated segregation of alloying elements such as Ni, Cr, Mo, and Mn at austenite grain boundaries in low alloy steels [24]. The difference in the atomic radii of Fe with Ni, Cr, and Mo are 0.007, 0.01, 0.034 nm, respectively [11]. The higher this difference, the higher is the tendency for segregation at austenite grain boundaries. Furthermore, adding Cr and Mo to this steel as alloying elements (Table 1), forms carbonitrides in austenite with high melting point and thus stability in the alloy (Fig. 2). They pin the austenite grain boundaries and decrease the growth rate of the austenite grain in the austenitization process.

In the investigated austenitization temperature and time ranges, no abnormal grain growth, *i.e.*, abrupt increase in the austenite grain size with increasing austenitization temperature or time, was observed. This is consistent with reported gradual growth of austenite grains in medium carbon steels as the austenitization temperature or time is increased [25]. This type of grain growth behavior is known as continuous or normal grain growth [14]. In contrast, in HSLA steels austenite grain growth behavior is different. These alloys contain microalloying elements like Nb, V, Ti, and Al (Al comes from the steel making process [13]), for refining grains through restricting austenite grain growth during reheating and impeding recrystallization during hot deformation by means of fine carbide precipitates of microalloying elements. In the HSLA steels, a rapid abnormal growth of austenite grains occurs due to dissolution of carbides formed by microalloying elements. For instance, Maropoulos et al. [26] observed such a behavior for a low-alloy steel containing 0.2 wt.% V. They reported that near the dissolution temperature of vanadium carbides (V_4C_3), *i.e.*, 1020 °C, abnormal grain growth, also known as discontinuous grain growth [14], was initiated. In this steel, the large number of vanadium carbides (V_4C_3) with a uniform distribution reduces the rate of grain boundary migration when the material is heated at temperatures below the dissolution temperature of the precipitates. In other words, the V_4C_3 precipitates stay effective for retarding or inhibiting austenite grain growth at austenitization temperatures below 1020 °C by applying strong pining effect on the grain boundaries. Therefore, abnormal austenite grain growth would not take place during thermal treatments at temperatures lower than 1020 °C for this Nb–V–Ti microalloyed steel and slight changes in the austenite grain size during austenitization would occur.

Particles size and volume fraction are important factors in pining grain boundaries and thus kinetics of grain growth. With increasing the austenitization temperature and time, the volume fraction of the particles decreases and their size increases. Therefore, the pinning force (F) caused by these particles decreases with increasing the austenitization temperature and time according to the following equation [3]:

$$F = C\gamma\frac{f}{r} \quad (1)$$

where C is a constant, γ is the grain boundary energy, f and r are the vol.% and the size (radius) of undissolved and coarsened particles, respectively. Consequently, growth of the austenite grains occurs during the austenitization process as the pinning force is reduced. In case of the microalloyed steel discussed above, once the vanadium carbides (V_4C_3) dissolve fully into austenite, at temperatures well above its dissolution temperature ($T > T_c$), rate of grain boundary migration rises quickly as there is no effective precipitates to pin the grain boundaries. These conditions provide the circumstances for

fast or abnormal grain growth. In summary, the complete dissolution of the precipitates during thermal cycles promotes abnormal grain growth. This is not desirable for the final refinement of the microstructure and resultant mechanical properties such as toughness and ductility. Hence, it is important to examine and control the grain growth in the industrial austenitization process for different steel grades by appropriate selection of austenitization temperature and time.

3.2. *Modeling austenite grain growth*

Based on a thermally activated atomic jump process, the following Arrhenius type constitutive equation is often used to explain the kinetics of the austenite grain growth in steel under isothermal austenitization conditions [2,27]:

$$d = [d_0^m + A\,t\exp(-\frac{Q}{RT})]^{\frac{1}{m}} \quad (2)$$

where d is the average grain size in μm, d_0 is the initial average grain size in μm before starting the austenitization, m is the inverse of the time exponent for grain growth, A is a constant, t is the austenitization time in second, Q is the activation energy for austenite grain growth in J/mol, R is the universal gas constant (8.314 J/(mol. K)), and T is the austenitizing temperature in Kelvin.

By taking the natural logarithm from both sides of Eq. (2), the m and Q parameters can be expressed as:

$$\frac{1}{m} = \left.\frac{\partial \ln d}{\partial \ln t}\right|_T \quad (3)$$

$$Q = -mR\left.\frac{\partial \ln d}{\partial (1/T)}\right|_t \quad (4)$$

The $\frac{1}{m}$ parameter is the slope of ln D-ln t graph and the Q parameter is equal to the slope of the ln d- ln $(1/T)$ graph times mR, as illustrated in Fig. 4. In this figure, the finest fit for every data set is also drawn to better identify the trends. It is evident that the austenite grain size can be estimated as a series of parallel and straight lines. Based on Fig. 4a, the austenite grain size increases with the austenitization time. In the same way, the austenite grain size increases with increasing the austenitization temperature, Fig. 4b. From the regression analysis using Eqs. (3) and (4), the n and Q values were calculated as 4.37 and 230.992 kJ/mol, respectively. The regression coefficients (R^2) for the above fits were 0.868 and 0.867, respectively, suggesting a proper linear relationship between ln d and ln t as well as ln d and ln $(1/T)$. It also points out a relatively good estimation of the experimental findings with the model.

The calculated activation energy is close to that (214 kJ/mol) reported by Khzouz [28] for steel grades with chemical compositions comparable to that of the present study. The calculated activation energy is also comparable to that for substitutional diffusion of transition alloying elements in a dilute solution of austenite (260 kJ/mol [23]) and the value for self-diffusion in pure austenite lattice (284 kJ/mol [23]). Therefore, austenite grain growth occurs by movement or diffusion of transition and self-iron atoms.

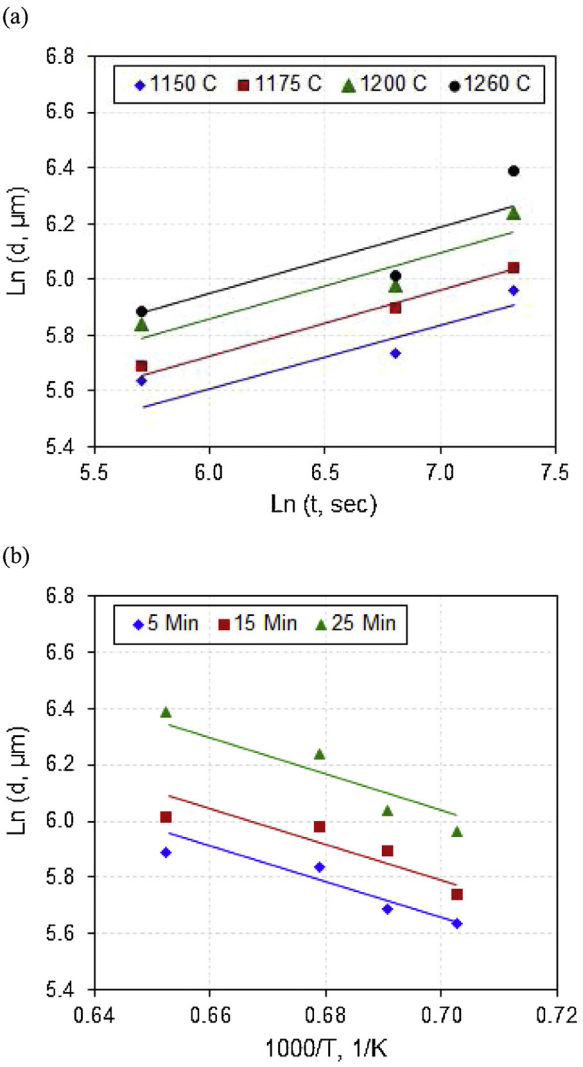

Fig. 4 – Variation of the average austenite grain size with (a) time and (b) reciprocal temperature in the austenitization process.

From the regression analysis of Eq. (2) in DEFORM® software [27], the A constant was calculated as 4.21435×10^{16}. Therefore, Eq. (2) can be rewritten as:

$$d = [d_0^{4.37} + 4.21435 \times 10^{16}\,t\exp(-\frac{230992}{RT})]^{\frac{1}{4.37}} \quad (5)$$

In Fig. 5, the experimental and predicted average austenite grain size using Eq. (5) are compared. A reasonable agreement between the experimental and predicted data can be observed for the studied austenitization temperature and time ranges. In particular, the average absolute relative error (E) between the experimental (d_E) and predicted (d_P) austenite grain size was calculated using the following equation:

$$E = \frac{1}{N}\sum_{i=1}^{N}\left|\frac{d_E^i - d_P^i}{d_E^i}\right| \times 100 \quad (6)$$

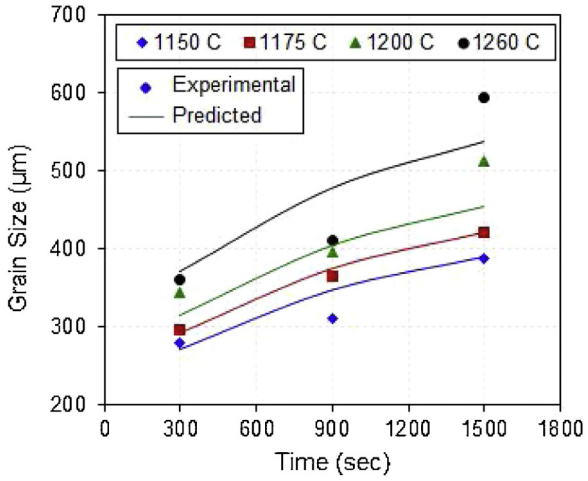

Fig. 5 – Comparison of the experimental and predicted average austenite grain size after austenitization using Eq. (5).

A similar equation is used by Chadha et al. [29] for determining error between experimental and predicted flow stresses during hot compression of a high strength steel. The error calculated using Eq. (6) was 6.0 %. Therefore, the grain growth behavior follows the Arrhenius relationship. The developed constitutive equation, Eq. (5), can effectively define the correlation between the austenite grain size, austenitization temperature, and time. In this way, the kinetics of the austenite grain growth for this type of steel and potentially many other commercial medium carbon low alloy steels under continuous heating and isothermal austenitization processes can be determined. As well, Eq. (5) developed in this study can be used as key input in finite element models for predicting the austenite grain growth during thermomechanical processing.

3.3. *Variation of flow stress with soaking time, deformation temperature, and strain*

The flow stress–strain curves attained under different soaking times at various hot compression temperatures at a fixed strain rate of 0.05 s^{-1} are plotted in Fig. 6 for the investigated steel. The flow behavior depends on the soaking time, deformation temperature, and strain to some extent. For all deformation temperatures (1150, 1175, and 1200 °C) and soaking times (5, 15, and 25 min), a typical DRX behavior was observed. This means the flow stress increased up to a distinct peak stress (σ_p) followed by a gradual decrease or softening toward a steady-state flow stress (σ_s) indicating DRX occurrence. The peak stress is very clear for the deformation temperatures of 1150 and 1175 °C and all soaking times. With increasing the deformation temperature to 1200 °C, for all soaking times the peak stress turns out to be wider, although the flow curves still represent a typical DRX curve as supported by observed dynamic softening or flow stress decrease after the peak stress. This implies that the flow stress increases initially and after slight softening it saturates gradually. In other words, at 1200 °C the amount of flow softening is reduced. In

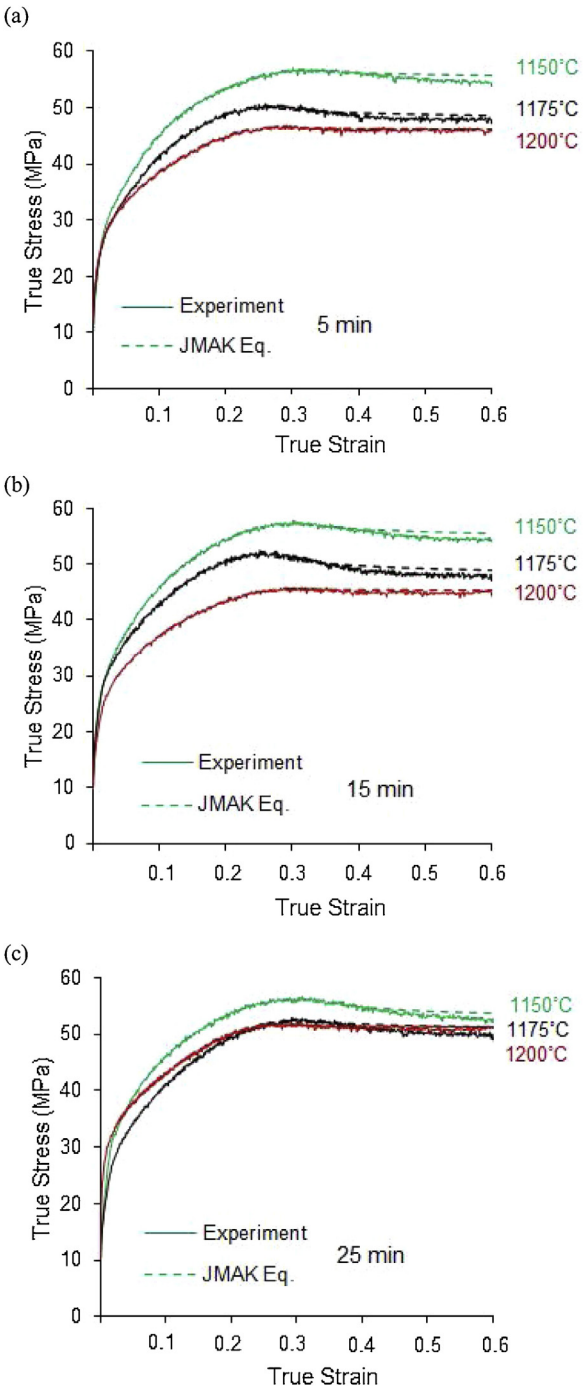

Fig. 6 – The experimental and predicted flow stress curves for different soaking times of (a) 5 min, (b) 15 min, and (c) 25 min and various hot compression temperatures.

summary, under any deformation condition in this study, the material exhibited a DRX type flow curve.

The dependency of the flow stress curves on the soaking time at the deformation temperature or simply austenite grain size prior to hot deformation is shown in Fig. 7 by plotting the curves for different soaking time at the same deformation temperature. For the deformation temperatures of 1150 °C, the flow curves are very similar for different soaking times (Fig. 7a). For the deformation temperatures of 1175 and 1200 °C,

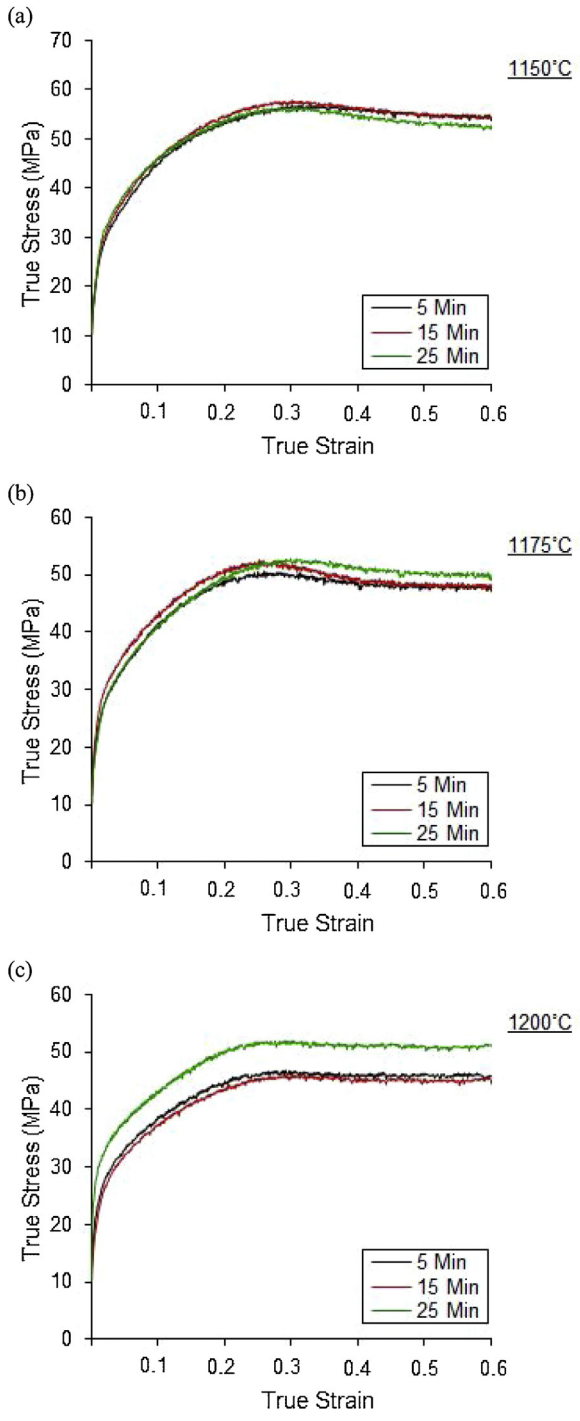

Fig. 7 – The experimental flow stress curves for different soaking times at various hot compression temperatures of (a) 1150 °C, (b) 1175 °C, and (c) 1200 °C.

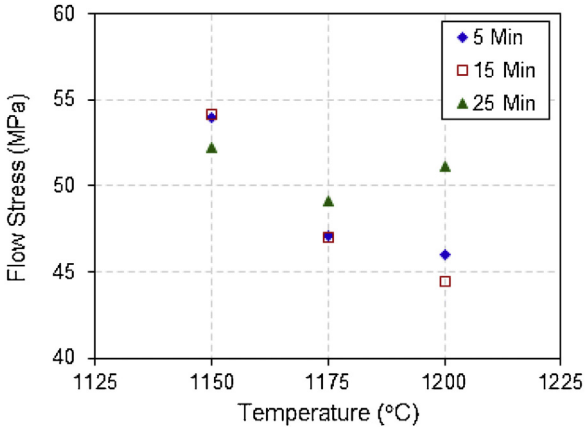

Fig. 8 – The variation of the flow stress at a true strain of 0.6 with the hot compression temperature for different soaking times at the deformation temperature.

for soak time of 5 and 15 min the flow curves are similar, however, with increasing the soak time to 25 min, the flow curve rises somewhat especially at 1200 °C. Therefore, it can be pointed out that the austenite grain size prior to hot deformation has almost negligible effect on the flow curves except for the deformation temperature of 1200 °C and soaking time of 25 min. The latter can be related to the coarsest austenite grain size (513 μm *vs.* ≤420 μm for other conditions) prior to hot deformation for 25 min and 1200 °C (Fig. 3a). In this way, less grain boundary area per unit volume is available for nucleation of DRXed grains and progress of DRX. Therefore, the flow stress curve has a higher level at 25 min and 1200 °C.

The dependency of the flow stress on the deformation temperatures and soaking time can be seen more evidently in Fig. 8. In this figure, the flow stress at a true strain of 0.6 is depicted as a function of the deformation temperature for different soaking times. At a specific soaking time, the flow stress decreases with increasing the deformation temperature, as anticipated, except for the deformation temperature of 1200 °C and soaking time of 25 min. The former behavior can be related to the enhancement in the mobility of dislocations and migration of grain boundaries and ease of softening occurrence by dislocation annihilation, DRV, and DRX at higher deformation temperatures. In other words, the softening mechanisms are thermally activated or diffusion-controlled processes [30]. For 1200 °C and 25 min, a very coarse prior austenite grain size along with interactions of solutes and particles with dislocations and grain boundaries contributes to the observed behavior.

Referring back to Fig. 6, in general, the competition between work-hardening and dynamic softening dictates the shape of the flow curves. At the early stage of deformation, severe dislocation generation rate and accumulation of dislocations result in work-hardening and relatively fast rise of flow stress. The extent of work-hardening is higher for lower deformation temperatures. With continuing the deformation, the dislocation density increases further leading to dynamic softening at high temperatures by DRV, *i.e.*, dislocation annihilation and rearrangement, and/or DRX at a critical strain. In this manner, dislocation density and interaction and thus work-hardening are reduced. So, the flow stress increases at a diminishing rate until the peak stress is reached. For the deformation temperature of 1200 °C and all soaking times, the flow softening after the peak stress is smaller compared to lower temperatures. However, almost for all hot deformation conditions, the flow softening is dominated indicating that after the peak stress with increasing strain, the dynamic softening rate surpasses the work-hardening rate. An almost steady-state flow stress

can be observed at a strain of ~ 0.5 for all conditions. A steady-state flow stress after the peak stress means the flow stress stays approximately constant and does not rise with strain. It is an indication of a dynamic balance between the work-hardening and the dynamic softening rates. In other words, at the steady-state flow stress dislocation generation and annihilation occur concurrently.

Deformation induced flow softening can be caused by various mechanisms like deformation (adiabatic) heating, enhanced DRV, subgrain coarsening, DRX, dynamic precipitation and dissolution, and coalescence/growth of precipitates [30]. Under the strain rate of 0.05 s^{-1} in the current study, the effect of adiabatic heating on the flow softening is negligible. This is consistent with other studies [19,31]. The impact of other mechanisms especially evolution of microstructure on the flow softening will be discussed in Section 3.8.

3.4. *Flow stress modeling*

Several authors [32–35] have used the following JMAK equation to describe the DRX kinetics:

$$X = 1 - \exp(-kt^n) \quad (7)$$

Where X is the DRX vol.%, k is the Avrami constant, t is the softening time, and n is the time exponent. The X parameter can be determined from the flow curves based on the following equation [17]:

$$X = \frac{\sigma_p - \sigma}{\sigma_p - \sigma_s} \quad (8)$$

In this equation, σ_p and σ_s were defined previously and σ is the flow stress at any point after the peak stress. The σ_p-σ represents the flow softening from peak to the flow stress of σ and σ_p-σ_s shows the maximum possible softening or softening between the peak and the steady-state stresses.

The softening time, t in Eq (7), can be determined from the following relationship [32]:

$$t = \frac{\varepsilon - \varepsilon_p}{\dot{\varepsilon}} \quad (9)$$

where ε is the strain, ε_p is the strain at the peak flow stress, and $\dot{\varepsilon}$ is the strain rate. By plotting $ln\ [ln\ (1-X)]$ versus $ln\ (t)$ at every deformation temperature, the k and n parameters in Eq (7) can be determined. The obtained values for k and n are provided in Table 2. From Eq.s (7),(8) and (9), the flow stress after the peak can be expressed as:

$$\sigma = \sigma_s + (\sigma_p - \sigma_s)\ exp[-k(\frac{\varepsilon - \varepsilon_p}{\dot{\varepsilon}})^n] \quad (10)$$

The dynamic softening part of the flow stress curves, *i.e.*, from the peak to the steady-state stress, was modeled using Eq (10). The predicted flow stress curves are compared with the measured ones in Fig. 6 for different hot deformation conditions. A good agreement between the predictions and experimental data can be observed for all cases. Therefore, the procedure for calculating the flow stress using Eq. (10) is a reliable approach for medium carbon low alloy steels under different hot deformation conditions.

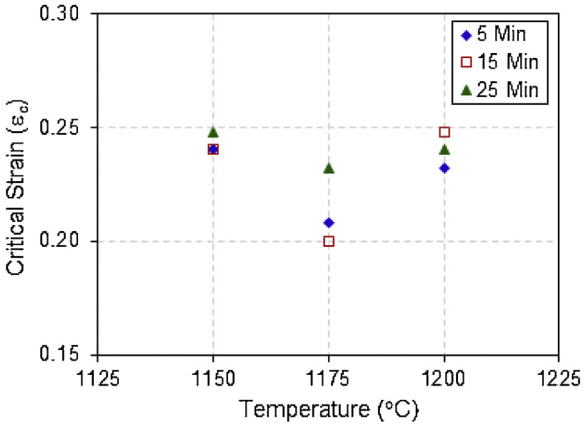

Fig. 9 – Variation of the critical strain (ε_c) with the hot deformation temperature for different soaking times at the deformation temperature.

3.5. *Variation of critical strain with prior austenite grain size and hot deformation conditions*

Critical strain (ε_c) is an important parameter in modeling of industrial hot deformation processes, since DRX initiates at ε_c, which is 0.6–0.8 times the strain (ε_p) at the peak flow stress (σ_p) [36]. In addition, DRX affects the high temperature flow behavior, microstructure evolution, and final mechanical properties. For a given alloy, initial grain size prior to hot deformation, temperature, and strain rate of deformation influence ε_c.

Fig. 9 demonstrates the variation of the critical strain (ε_c) for the onset of DRX with the deformation temperature for different soaking times. To plot this graph the $\varepsilon_c = 0.8\ \varepsilon_p$ equation was taken into account [31,37]. Overall, the critical strain for onset of DRX lies in the 0.20–0.25 range under the investigated conditions. This means DRX can be initiated at a small strain under these hot deformation conditions. A soaking time of 15 min and a deformation temperature of 1175 °C offers the lowest ε_c and thus, the easiest condition for DRX initiation. Based on Fig. 9 the strain for onset of DRX varies somewhat with soaking time (initial grain size prior to hot deformation) and the deformation temperature. Almost for every soaking time, by increasing the deformation temperature the critical strain decreases to some extent initially and then rises slightly. The former behavior can be related to the enhancement in the mobility of dislocations and grain boundaries with increasing deformation temperature and needing a smaller critical strain for onset of DRX. The latter behavior is most likely associated with the coarser prior austenite grain size as well as the interactions of solutes and particles with dislocations and grain boundaries.

3.6. *Extent of flow softening*

For different hot deformation conditions in the current study, the extent of the flow softening was calculated based on the $\frac{\sigma_p - \sigma_{0.6}}{\sigma_p} \times 100$ expression, where $\sigma_{0.6}$ is the flow stress at a true strain of 0.6. Fig. 10 shows the calculated values as a function of the deformation temperature for different soaking times. For 5 and 15 min soaking times, the amount of flow soften-

Table 2 – The determined values for *k* and *n* parameters for various soaking times at different hot compression temperatures.

	k			*n*		
Time (min)/Temperature (°C)	1150	1175	1200	1150	1175	1200
5	0.369	0.457	1.146	0.533	0.530	0.229
15	0.439	0.482	0.607	0.658	0.660	0.278
25	0.417	0.400	0.952	0.800	0.577	0.338

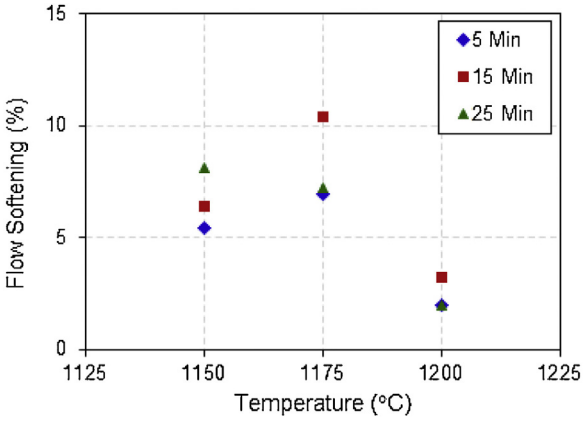

Fig. 10 – Variation of the flow softening extent with the hot deformation temperature for different soaking times.

ing increased initially and then decreased with increase of the deformation temperature. In contrast, for the 25 min soak time, a decreasing trend was observed. Overall, for the investigated conditions the amount of flow softening was ~10% or less.

3.7. *Determination of DRX kinetics from flow curves*

As inferred from flow curves (Fig. 6), DRX is the main softening mechanism in the investigated steel. It is easier to determine the DRX vol. % (X) from the flow curves than the microstructure analysis. Neglecting the impact of the DRV on the flow softening, the DRX vol.% has direct relationship with the flow softening [17]. The DRX kinetics calculated as X or the calculated DRX vol.% is depicted as a function of strain in Fig. 11 using Eq (8). In this figure, the impact of the soaking time (or initial grain size prior to hot deformation), hot compression temperature, and strain at a fixed strain rate of 0.05 s^{-1} on the DRX vol.% can be realized. The onset of DRX was considered at ε_c, *i.e.*, for every hot deformation condition $X = 0$ at ε_c.

Overall, DRX consists of three phases: (i) incubation at the beginning, (ii) increase of kinetics or acceleration, and (iii) steady-state. Also, for a given soaking time and deformation temperature, DRX vol.% increases with increasing strain reaching the 100 % value or complete DRX easily at the end which indicates attaining a steady-state flow stress. The increase in the DRX vol. % with strain can be related to the nucleation and growth of more DRXed grains.

In Fig. 11a, the impact of the soaking time at a fixed midrange deformation temperature of 1175 °C is illustrated as a representative example. As can be inferred from Fig. 3b, at a given temperature, with increasing the soaking time the

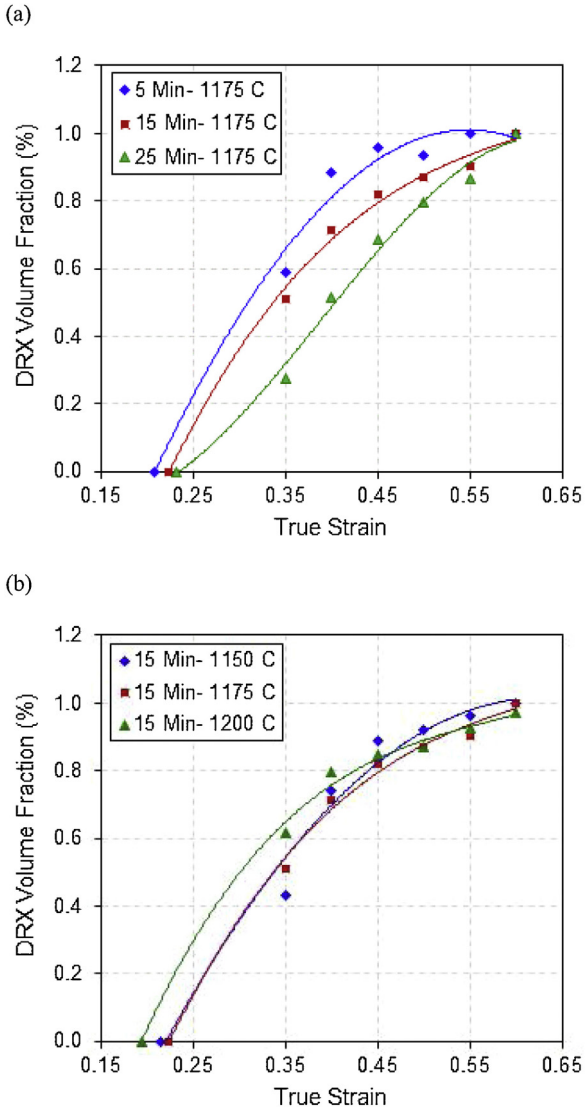

Fig. 11 – The calculated DRX vol.% as a function of the true strain for (a) different soaking times at a fixed 1175 °C hot compression temperature and (b) a fixed soaking time of 15 min and different hot compression temperatures.

grain size increases. In other words, grains prior to hot deformation become coarser with increasing the soaking time at the deformation temperature. This means less grain boundary area per unit volume is available for nucleation of DRXed grains and advancement of DRX. Therefore, the DRX kinetics become slower with increasing the soaking time (Fig. 11a). Moreover, with increasing the soaking time, a higher strain is

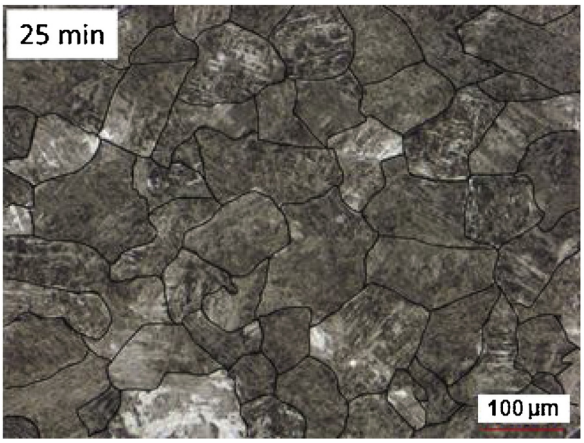

Fig. 12 – The hot compressed microstructure after soaking for 25 min at the 1150 °C and applying a true strain of 0.6 at this temperature.

required to attain the same level of DRX. The same situation exists for the steady-state deformation, *i.e.,* the strain necessary for the steady-state deformation increases as the soaking time is increased.

In Fig. 11b the effect of the deformation temperature on the DRX kinetics at a fixed midrange soaking time of 15 min is depicted. The DRX kinetics is accelerated at a higher deformation temperature as DRX is a thermally activated process. This is the case for a 1200 °C deformation temperature compared with 1150 and 1175 °C for considerable part of the investigated strain range, *i.e.,* up to a strain of 0.46.

3.8. *Microstructure evolution during hot compression*

In materials with low stacking fault energy (SFE) such as austenite in steel, the DRV is sluggish and work-hardening is not balanced by DRV. Hence, once a critical strain is exceeded resulting in adequate accumulation of dislocations, DRX will be initiated. The microstructure of the investigated steel after isothermal hot compression under different conditions to a true strain of 0.6 were investigated. A micrograph corresponding to that in Fig. 2 is shown in Fig. 12, as a representative example. The DRX process is initiated and completed for all deformation conditions as supported by the following quantitative grain size data. The original coarse grains after austenitization (Fig. 2) are replaced entirely by new finer, uniform, and equiaxed DRXed grains (Fig. 12). Therefore, hot deformation processes such as hot forging in which DRX is operative are effective in refining and controlling the coarse prior austenite grain structure in medium carbon low alloy steels. In addition, DRX occurrence provides good workability through concurrent softening, and the associated microstructure regeneration prevent formation of unstable microstructural features such as grain boundary cracking/cavitation or shear bands caused by strain buildup. So, the microstructures of the studied steel can be restored by hot deformation, which results in improved hot workability and mechanical properties.

Table 3 – The average austenite grain sizes after soaking for various times at different hot compression temperatures and then applying a true strain of 0.6.

Time (min)	Temperature (°C)		
	1150	1175	1200
5	64	62	62
15	74	63	67
25	66	67	92

From quantitative grain size perspective, prior to hot compression the microstructure exhibited equiaxed coarse grains with an average size in the 280–595 μm range (Fig. 3a) as a result of austenitization under different temperatures and times. The average austenite grain size data after hot compression, *i.e.,* the average steady-state austenite grain size, are shown in Table 3 for different hot deformation conditions. Based on this table and micrographs (Figs. 2 and 12), after hot compression, the size of the grains is substantially reduced. In particular, more or less the DRX grain size and microstructures are similar with a grain size of ~ 66 μm on average, except for 25 min and 1200 °C. For the latter, as the deformation temperature is increased to 1200 °C coarsening of the DRXed grains has taken place as evidenced by a grain size of 92 μm. The increase of the deformation temperature to 1200 °C enhances the ability of the grain boundary migration and stimulates the growth of the DRXed grains. This 92 μm grain size might not be desirable as a coarse grain size can deteriorate mechanical properties. Accordingly, the hot deformation of this steel should not be carried out at the processing conditions corresponding to the microstructure generating a grain size of 92 μm, *i.e.,* austenitization at 1200 °C for 25 min, and then hot deformation at 1200 °C to a true strain of 0.6 at a strain rate of 0.05 s^{-1}. In other words, this condition is the upper limit of the hot working window for this steel. Therefore, with controlling the DRX by regulating the processing parameters such as austenitization temperature and time as well as deformation temperature, strain rate, and strain level the desired grain size and mechanical properties can be attained.

The DRX occurrence under the investigated conditions agrees well with the evolution of flow curves. The softening caused by DRX promotes a declining flow curve and creates a peak flow stress before attaining a steady-state stress. Indeed, softening after the peak stress is due to the progress of DRX. Consistently, achieving the fine equiaxial grains is a sign of reaching the steady-state situation. This means at the steady-state strain corresponding to the beginning of the steady-state flow stress full DRX is attained.

4. Conclusions

The austenite grain growth kinetics during isothermal austenitization in the 1150–1260 °C temperature range for soaking times in the 5–25 min range in a medium carbon low alloy forged steel were studied. Also, an Arrhenius relationship for prediction of the austenite grain growth was developed. In addition, the hot deformation behavior and microstructure development during the subsequent isothermal compression in the 1150–1200 °C temperature range and strain rate of 0.05

s^{-1} were investigated. An empirical model for the prediction of the flow stress curve after the peak was established. As well, the DRX kinetics were determined from the flow curves. The following conclusions can be drawn from this study:

1 A normal or continuous austenite grain growth was observed. The austenite grain size increased gradually with increasing the austenitization temperature and time.
2 The constitutive equation for isothermal austenite grain growth was developed as $d = [d_0^{4.37} + 4.21435 \times 10^{16}\, t \exp(-\frac{230992}{RT})]^{\frac{1}{4.37}}$ with a 230.992 kJ/mol activation energy for grain growth. The predicted grain growth kinetics for different austenitization temperatures and times were in good agreement with the experimental data.
3 The flow stress curves displayed a typical DRX behavior including initial rapid work-hardening up to a peak stress, followed by softening toward a steady-state stress. In other words, DRX was responsible for flow softening during hot compression. The developed model for prediction of the flow stress curve as a function of strain for different hot deformation conditions was effective with negligible errors.
4 The critical strain for the onset of DRX was relatively small ($\leq$ 0.25) for the investigated hot deformation conditions. DRX kinetics was accelerated by increasing strain and deformation temperature as well as reducing the soaking time or prior austenite grain size. At a true strain of 0.6 the microstructure was fully DRXed for different prior austenite grain sizes and deformation temperatures and resulted in the formation of fine and equiaxed grain structures.
5 Relatively coarse grain size (280−595 μm) attained after austenitization was significantly refined down to 62–92 μm by DRX occurrence during hot deformation. As the hot deformation temperature was increased from 1150−1175 °C range to 1200 °C, the DRXed grains coarsened from ~ 66 μm to 92 μm.

Conflicts of interests

The authors declare no conflicts of interest.

Data availability

The raw/processed data required to reproduce these findings cannot be shared at this time as the
data also forms part of an ongoing study.

REFERENCES

[1] Sun HM, Li MQ, Liu YG. Development of processing map coupling grain size for the isothermal compression of 300 M steel. Mater Sci Eng A 2014;595:77–85.
[2] Zhang SS, Li MQ, Liu YG, Luo J, Liu TQ. The growth behavior of austenite grain in the heating process of 300M steel. Mater Sci Eng A 2011;528:4967–72.
[3] Yang G-W, Sun X-J, Yong Q-L, Li Z-D, Li X-X. Austenite grain refinement and isothermal growth behavior in a low carbon vanadium microalloyed steel. J Iron Steel Res Int 2014;21(8):757–64.
[4] Chentouf SM, Jahazi M, Lapierre-Boire L-P, Godin S. Characteristics of austenite transformation during post forge cooling of large-size high strength steel ingots. Metallogr Microstruct Anal 2014;3:281–97.
[5] Teng L, Guo C, Wang LZ. Constitutive modelling and microstructure evolution of 40Cr alloy steel during hot compression deformation. Mater Res Innov 2013;17(sup1):135–43.
[6] Duan L-N, Wang J-M, Liu Q-Y, Sun X-J, Cao J-C. Austenite grain growth behavior of X80 pipeline steel in heating process. J Iron Steel Res Int 2010;17(3):62–6.
[7] Sha Q, Sun Z. Grain growth behavior of coarse-grained austenite in a Nb–V–Ti microalloyed steel. Mater Sci Eng A 2009;523:77–84.
[8] Fujita N, Narushima T, Iguch Y, Ouchi C. Grain refinement of as cast austenite by dynamic recrystallization in HSLA steels. ISIJ Int 2003;43(7):1063–72.
[9] Maalekian M, Radis R, Militzer M, Moreau A, Poole WJ. In situ measurement and modelling of austenite grain growth in a Ti/Nb microalloyed steel. Acta Mater 2012;60:1015–26.
[10] Zhang L, Kannengiesser T. Austenite grain growth and microstructure control in simulated heat affected zones of microalloyed HSLA steel. Mater Sci Eng A 2014;613:326–35.
[11] Lee S-J, Lee Y-K. Prediction of austenite grain growth during austenitization of low alloy steels. Mater Des 2008;29:1840–4.
[12] Yu Q, Sun Y. Abnormal growth of austenite grain of low-carbon steel. Mater Sci Eng A 2006;420:34–8.
[13] Fernández J, Illescas S, Guilemany JM. Effect of microalloying elements on the austenitic grain growth in a low carbon HSLA steel. Mater Lett 2007;61:2389–92.
[14] Chen RC, Hong C, Li JJ, Zheng ZZ, Li PC. Austenite grain growth and grain size distribution in isothermal heat-treatment of 300M steel. Procedia Eng 2017;207:663–8.
[15] Liu YG, Liu J, Li MQ. The study on kinetics of static recrystallization in the two-stage isothermal compression of 300M steel. Comput Mater Sci 2014;84:115–21.
[16] Xu Y, Tang D, Song Y, Pan X. Prediction model for the austenite grain growth in a hot rolled dual phase steel. Mater Des 2012;36:275–8.
[17] Wei H-L, Liu G-Q, Xiao X, Zhang M-H. Dynamic recrystallization behavior of a medium carbon vanadium microalloyedsteel. Mater Sci Eng A 2013;573:215–21.
[18] Ebrahimi GR, Arabshahi H, Javdani M. Hot deformation behavior of Nb–V microalloyed steel. J Mech Eng Res 2010;2(5):92–6.
[19] Chamanfar A, Valberg HS, Templin B, Plumeri JE, Misiolek MZ. Development and validation of a finite-element model for isothermal forging of a nickel-base superalloy. Materialia 2019;6:100319.
[20] Kim SI, Lee Y, Byon SM. Study on constitutive relation of AISI 4140 steel subject to large strain at elevated temperatures. J Mater Process Technol 2003;140:84–9.
[21] Momeni A, Abbasi SM, Badri H. Hot deformation behavior and constitutive modeling of VCN200 low alloy steel. Appl Math Model 2012;36:5624–32.
[22] Wei H-L, Liu G-Q, Xiao X, Zhao H-T, Ding H, Kang R-M. Characterization of hot deformation behavior of a new microalloyed C–Mn–Al high-strength steel. Mater Sci Eng A 2013;564:140–6.
[23] Uhm S, Moon J, Lee C, Yoon J, Lee B. Prediction model for the austenite grain size in the coarse grained heat affected zone of Fe–C–Mn steels: considering the effect of initial grain size on isothermal growth behavior. ISIJ Int 2004;44(7):1230–7.
[24] Papworth AJ, Williams DB. Segregation to prior austenite grain boundaries in low-alloy steels. Scr Mater 2000;42:1107–12.

[25] Lee CS, Lee KA, Li DM, Yoo SJ, Nam WJ. Microstructural influence on fatigue properties of a high-strength spring steel. Mater Sci Eng A 1998;241(1–2):30–7.
[26] Maropoulos S, Karagiannis S, Ridley N. The effect of austenitising temperature on prior austenite grain size in a low-alloy steel. Mater Sci Eng A 2008;483–484:735–9.
[27] DEFORM®-3D version 11.2. Columbus, Ohio: Scientific Forming Technologies Corporation (SFTC); 2019.
[28] Khzouz E. Grain growth kinetics in steels. Mechanical Engineering, Worcester Polytechnic Institute; 2011.
[29] Chadha K, Shahriari D, Tremblay R, Bhattacharjee PP, Jahazi M. Deformation and recrystallization behavior of the cast structure in large size, high strength steel Ingots: experimentation and modeling. Metall Mater Trans A 2017;48A(September):4297–313.
[30] Chamanfar A, Alamoudi MT, Nanninga NE, Misiolek MZ. Analysis of flow stress and microstructure during hot compression of 6099 aluminum alloy (AA6099). Mater Sci Eng A 2019;743:684–96.
[31] Chamanfar A, Jahazi M, Gholipour J, Wanjara P, Yue S. Evolutionof flow stress and microstructure during isothermal compression of Waspaloy. Mater Sci Eng A 2014;615:497–510.
[32] Jonas JJ, Quelennec X, Jiang L, Martin E. The Avrami kinetics of dynamic recrystallization. Acta Mater 2009;57:2748–56.
[33] Shafaat MA, Omidvar H, Fallah B. Prediction of hot compression flow curves of Ti–6Al–4V alloy in alpha +beta phase region. Mater Des 2011;32:4689–95.
[34] Mirzadeh H, Najafizadeh A. Extrapolation of flow curves at hot working conditions. Mater Sci Eng A 2010;527:1856–60.
[35] Sarkar A, Chakravartty JK. Investigation of progress in dynamic recrystallization in two austenitic stainless steels exhibiting flow softening. Int J Metall Eng 2013;2(2):130–6.
[36] Wei H-L, Liu G-Q, Zhao H-T, Zhang M-H. Effect of carbon content on hot deformation behaviors of vanadium microalloyed steels. Mater Sci Eng A 2014;596:112–20.
[37] Shen G, Semiatin SL, Shivpuri R. Modeling microstructural development during the forging of Waspaloy. Metall Mater Trans A 1995;26A:1795–803.